Anuário do Instituto de Geociências - UFRJ
www.anuario.igeo.ufrj.br

Study of Radarfacies in Auriferous Placers at Baixada Cuiabana, Mato Grosso (Brazil)

Estudo de Radarfacies em Placeres Auríferos na Baixada Cuiabana, Mato Grosso (Brasil)

Maria Clara Lopes Paula; Welitom Rodrigues Borges & Isabela Resende Almeida

Universidade de Brasília, Instituto de Geociências, Programa de Pós-Graduação em Geociências Aplicadas e Geodinâmica, Campus Darcy Ribeiro, 70910-900, Asa Norte, Brasília, DF, Brasil
E-mails: mariaclara.lopespaula@gmail.com; welitom@unb.br; isabelaresalme@gmail.com
Recebido em: 20/03/2020 Aprovado em: 20/07/2020
DOI: http://doi.org/10.11137/2020_3_84_97

Resumo

O estado do Mato Grosso é o quinto maior produtor de ouro no Brasil, com boa parte da produção proveniente da região da Baixada Cuiabana. Nesta região, o ouro ocorre em depósitos primários associado a veios de quartzo e suas encaixantes, rochas metassedimentares do Grupo Cuiabá, e depósitos sedimentares secundários (como colúvios, alúvios e elúvios), sendo estes últimos bastante rentáveis e de fácil exploração. A explotação de ouro nestas áreas muitas vezes acarreta o desmatamento do bioma do Pantanal, pois a atividade minerária utiliza de escarificação aleatória do subsolo para localização dos depósitos. Neste estudo, testou-se o método geofísico de Radar de Penetração no Solo (GPR) na diferenciação e localização de depósitos aluvionares, coluvionares e eluvionares, para, por consequência, ajudar na mitigação do processo de desmatamento local. As aquisições de dados de GPR aconteceram em um garimpo localizado no município de Nossa Senhora do Livramento. Os registros de GPR ocorreram com antena blindada de 200 MHz, ao longo de cavas e exposições de cascalhos. Os resultados mostram a onda eletromagnética no meio variando entre 0,085 e 0,146 m/ns, ou entre -0,8 e 0,8, tomando-se amplitudes normalizadas de -1 a 1. Os menores valores de velocidade foram identificados nos cascalhos considerados de origem aluvionar. A velocidade intermediária de 0,090 m/ns associa-se a elúvios e a maior velocidade (0,146 m/ns) ao cascalho tido como de origem coluvionar. O GPR mostrou-se eficiente para distinguir depósitos sedimentares secundários auríferos na Baixada Cuibana, tornando-se uma alternativa prospectiva para a região.

Palavras-chaves: *Radar de Penetração no Solo; Depósitos Secundários; Geofísica*

Abstract

The state of Mato Grosso (MT) is the fifth largest gold producer in Brazil, with much of it coming from the Baixada Cuiabana region. In this region, gold occurs in primary deposit associated with quartz veins and their host metasedimentary rocks of the Cuiabá Group and secondary sedimentary deposits (such as colluviums, alluviums and eluviums), the latter being quite profitable and easy to exploit. The gold exploitation in these areas often results in deforestation of the Pantanal biome, as mining uses random subsoil scarification to locate the deposits. In this study, the Ground Penetrating Radar (GPR) geophysical method was applied to differentiate and locate alluvial, colluvial and eluvial deposits. This may help to mitigate the local deforestation process. Thus, the acquisition of GPR data took place in a gold mine located in the municipality of Nossa Senhora do Livramento. The GPR recordings were done with a 200 MHz shielded antenna, along with ditches and gravel exposures. The results show variability of the electromagnetic wave velocity between 0.085 to 0.146 m/ns, with normalized amplitudes of -1 to 1 ranging between maximum values of -0.8 and 0.8. The lowest velocity values were found for gravels of alluvial origin. The intermediate velocity of 0.090 m/ns is associated with eluviums and the highest velocity (0.146 m/ns) is associated with gravel of colluvial origin. GPR was efficient to distinguish secondary sedimentary deposits in the Baixada Cuibana, becoming a prospective alternative for the region.

Keywords: *Ground Penetration Radar; Secondary Deposits; Baixada Cuiabana*

Anuário do Instituto de Geociências - UFRJ
ISSN 0101-9759 e-ISSN 1982-3908 - Vol. 43 - 3 / 2020 p. 84-97

1 Introduction

Although the largest gold exploitation comes from large miners, a significant amount of gold is also produced by small artisanal miners, both legally and illegally; reaching great economic expression in some countries (Ferreira Filho, 2019). However, despite the country's economic development due to mineral exploration, mining and metallurgy activities, they are recognized as having a high environmental impact. In Brazil, the mining and metallurgy sectors have only recently begun to invest in development and adoption of new technologies, to reduce the impacts caused by their activities. According to 2017 National Bank for Economic and Social Development - BNDES data, new technologies are being adopted to optimize control, automate operations, enable new mining and transformation enterprises. In this context, interest in the use of non-invasive geophysical techniques in mineral exploration arises.

In Brazil, the Mato Grosso state was the fifth largest gold producer in 2018 (Ferreira Filho, 2019). One of its golds producing regions is located in the Baixada Cuiabana region, where prospecting and mining activities are performed by small companies. Often, due to lack of interest in new techniques, they use faster and less costly methods for locating gold deposits, such as random scarification of the subsoil, with total removal of Cerrado vegetation cover. This causes several types of impacts in Pantanal's biome. With environmental damage and scarcity of apparent deposits, the need for non-invasive techniques that map the subsurface with relative efficiency and low operating cost becomes even greater given the increased demand for ores and environmental preservation. Over the past 25 years, new applications have emerged for the Ground Penetrating Radar (GPR) method, ranging from archeology to the substrate mapping of the planet Mars. In 1984 works such as Davis & Vaughan (1984) already showed the applicability of GPR in mining, highlighting the need for more compact and robust equipment for studies. In Watts & Gubins (1997) there were some experiments with electromagnetic waves in nickel deposits, where it was observed that the occurrence depths of this transition metal presented a challenge for geophysical methods. However, only recently that GPR has been applied and has shown good results in mining (Francké & Yelf, 2003). This method has been used in large scale for preliminary exploration of areas with potential for mining, as well as in local scale for three-dimensional reconstruction of subsurface structures (Francké & Yelf, 2003). Many works such as those presented in Huggenberger & Pugin(1994); Beres *et al.* (1995); Vandenberghe, & Overmeeren (1999); Regli & Rauber (2002); Heinz *et al.* (2003); Neal (2004); Kostic *et al.* (2005); Bersezio *et al.* (2007); Engdahl & Bonal (2010); Calder & Kennedy (2013); and Pueyo Anchuela *et al.* (2016) discuss the efficiency of the ground penetration radar geophysical method in the characterization and measurement of soil gravel deposits from different sources. Statistical analysis was carried out based on works like Rauber *et al.* (1998); Regli *et al.* (2002); Chen *et al.* (2004); Moysey *et al.* (2006) and Tebchrany *et al.* (2014) that exhibited GPR data assimilation techniques with statistical methods.

In this context, this paper intended to investigate the capacity of the GPR method to identify and recognize alluvial, eluvial and colluvial deposits, which have a high potential for host gold occurrences in the study area. Another objective of this paper is to observe the extension of the relations between: lithologies, different reflection patterns, amplitude statistics on each reflection pattern, and calculations of the particular electromagnetic wave velocities in each lithology may be relevant for the discretization of these deposits.

1.1 Geological Context

The Baixada Cuiabana region is located in the Neoproterozoic Paraguay Belt, which surrounds the southwestern edge of the Amazonian Craton, and comprises essentially folded and metamorphosed sedimentary rocks (Alvarenga & Trompete, 1993). The main geological unit is the Cuiabá Group (Luz *et al.*, 1980), which comprises NE-trending low-grade metasedimentary rocks such as graphite-rich, pyritic or carbonate-rich phyllites, as well as metarenites, metaconglomerates, quartzites and marbles with ages ranging from Neoproterozoic to Cambrian (Barboza, 2008). This Group is subdivided by Luz *et al.* (1980) in eight subunits, where two of them appears in this study area (subunit 3 and 5). There, subunit 3 is composed of phyllites, metaconglomerates, metarkoses and metarenites locally ferruginous, calciferous phyllite lenses and hematite levels at the top; while the subunit 5 is composed of phyllites, metarkoses, metaconglomerates and subordinate quartzites (Figure 1) (Luz *et al*.,1980).

The gold occurrences in the Cuiabá Group are related to the sedimentary protolith (clastic origin) or concentrated in quartz veins that cross-cut metasedimentary units of hydrothermal origin (Pires *et al.*, 1986; Silva *et al.*, 2016). In addition, gold occurs in lateritic sedimentary covers, which are resulted of supergenic processes, related to the evolution of lateritic eluvial covers on lithologies previously mineralized (Del'Rey Silva, 1990). In the municipality of Nossa Senhora do Livramento, gold was initially mined in alluvial and lateritic deposits (Fernandes & Miranda, 2006). With the intense exploitation, primary deposits were also exposed (Fernandes & Miranda, 2006). Hence, the quartz veins and their hosting rocks, belonging to the Cuiabá Group, commenced to be explored (Fernandes & Miranda,

2006). The miner's records in the region indicate high gold percentages in eluvial gravels, followed by colluvium and finally the alluvium. However, despite the higher levels found in the eluvium, they prefer to mine in alluvial gravely beds due to their greater thickness and, consequently, their greater volume.

Thus, this project takes place inside a small gold mining at Nossa Senhora do Livramento. Geographic information system (GIS) data, and the Cuiabá Group sedimentary rocks NE/EW orientation were used to locate the survey lines (Figure 1). Figure 1A display the simplified geological map study area, its gold deposits and the locations of the recognized gravely levels of interest. Figure 1B indicate the GPR survey lines arrangement, preferably parallel to the gravely levels direction, aiming to map its continuity; the location of the three inspected gravely levels mapped by them; and the alluvial terraces area deposits recognized with GIS and surrounded by the area which do Couto & Saes (2008) defined as the Cuiabá Group Acorizal Formation.

Moreover, the survey profiles orientation was mainly guided by *in situ* visual recognition of eluvial, colluvial and alluvial gravely layers nearby its mining exploration areas (Figure 2 and Table 1). Figure 2 summarizes the gravely layers distribution within a hypothetical topography and geomorphology. Table 1 detailed the main characteristics sought in the *in-situ* recognition of eluvial, colluvial, and alluvial gravely layers.

2 Methodology

The study area is located inside a small gold mining at Nossa Senhora do Livramento, at Baixada Cuiabana region. In this area, the Ribeirão dos Cocais drainage was the location of intense gold exploitation due to the presence of alluvial deposits in its active bed. In the time of this study's GPR data acquisition, this mining extracted gold from the metasedimentary rocks, the quartz veins, and the lateritic eluvial covers, as shown by the remnant open pits in Figure 1B. There, the NE/EW sedimentary rocks orientation is an

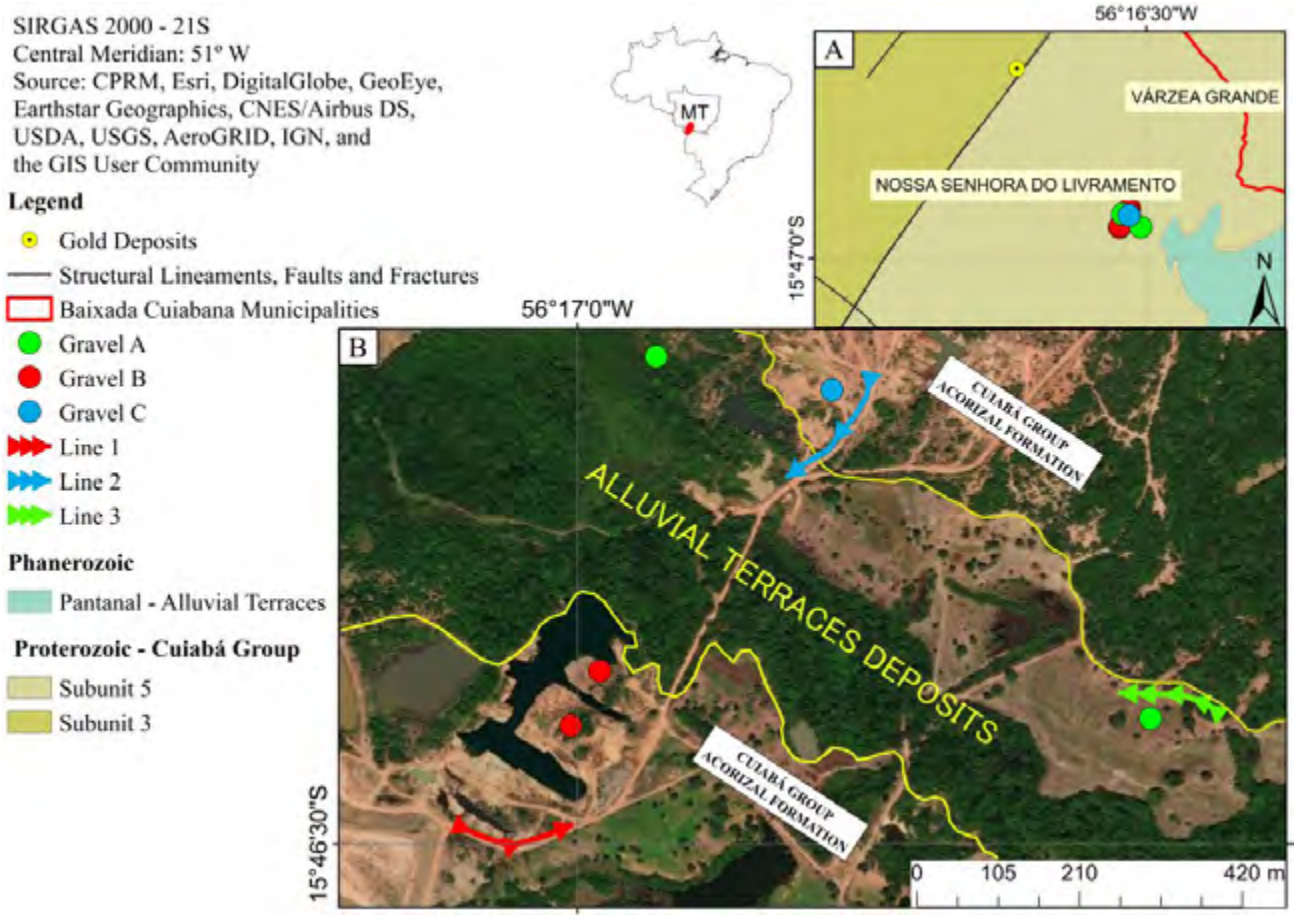

Figure 1 A. Geological map of the study area in the municipality of Nossa Senhora do Livramento near its limit with Várzea Grande and its situation in the Mato Grosso state; B. Satellite image showing the alluvial terraces deposits area surrounded by Cuiabá Group Acorizal Formation, the placement of gravels A, B and C, and finally the data acquisition arrangement for lines 1, 2 and 3.

Anuário do Instituto de Geociências - UFRJ
ISSN 0101-9759 e-ISSN 1982-3908 - Vol. 43 - 3 / 2020 p. 84-97

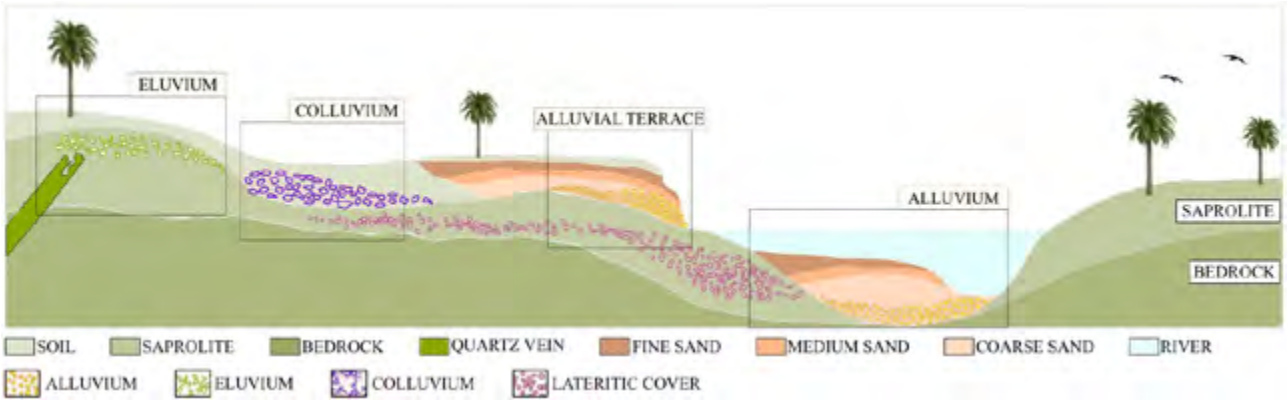

Figure 2 Illustration of eluvium, colluvium, alluvial terrace and alluvium secondary deposits distribution within a given hypothetical topography and morphology.

Eluvium	Colluvium	Alluvium
Deposit composed of weathered material that remains still or nearby its source area. It's mainly formed of coarse and angulous clasts, where the low density materials are commonly removed.	Deposit composed of loose, unconsolidated, weathered material that have been deposited by rain-wash, sheetwash, or other gravity process. Its formed by heterogeneous rocks, poorly selected, ranging from silt to cobbles or boulders.	Deposit composed of loose and unconsolidated detritic material that has been transported by a river and redeposited along its pathway, either in the riverbed or on its floodplain. It's mainly composed of fine particles of silt and clay together with larger and commonly rounded particles of sand and gravel.

Table 1 Main characteristics sought in the *in-situ* recognition of eluvial, colluvial, and alluvial gravely layers illustrated by Figure 2

obvious prospective advisor to find mineralized quartz veins and their related secondary deposits. Hence, gravely levels presenting the main characteristics of eluvial, colluvial and alluvial deposits (Table 1) were recognized *in situ*, in order to orient the GPR line surveys along its continuity, aiming to map its texture as long as possible. Figure 3 shows detailed photographs of the main gravely layers with the required characteristics of secondary deposits located in their respectively areas pointed by Figure 2; A. a matrix-supported, fine and well selected gravel, interspersing fine particles with larger and rounded particles, where A1 is gray colored probably due to the presence of hematite, as pointed by Luz *et al.* (1980) in subunit 3, and A2 is yellow, perhaps due to the presence of goethite; B. a matrix-supported and poorly selected gravel, mainly formed by coarse and angulous clasts; and; C. a matrix-supported, angulous and poorly selected gravel, ranging from silt to cobbles.

To acquire the 2D GPR profiles presented in this work, equipment from the Geography Department of the University of Brasilia was used, as follows: an SIR 3000 (GSSI) system coupled to the 200 MHz shielded antenna accompanied by an odometer to activate the trigger. To ascertain the wave's medium velocity, a flat iron bar was buried at a depth of 0.50 m (Figure 4A). The double travel time shown in the radar profile time scale for the electromagnetic wave reflecting path on this target was 13.236 ns and the wave medium velocity found, 0.074 m/ns (radargram shown in Figure 4B).

In this study, the GPR profiles were submitted to a processing sequence to reduce the noises and emphasize the reflectors of interest, maintaining the initial signal response as much as possible. These procedures were performed in ReflexW software, version 7.5 (Sandmeier, 2011), and follow the order illustrated by Figure 5.

The processing steps were made with the following objectives: the time-zero correction involved setting as the time-zero position the airwave first amplitude positive peak on the first trace; dewow subtraction has been applied to remove low frequency components from the data which are associated with electronic saturation of the receiver; background removal served to remove systematic air wave related noise; header gain removal was utilized to retrieve original amplitude information, being useful for further statistical comparisons of original amplitude information; and the manual y gain was last applied to emphasize responses along the y axis with an interactive gain of 10 dB starting in 5 ns.

After processing, a correlation was generated between the resulted radargrams and open excavations in the field. In these lines, the depths of the gravely levels were estimated from the velocities observed in the profiles with the ReflexW program (Sandmeier, 2011); from this

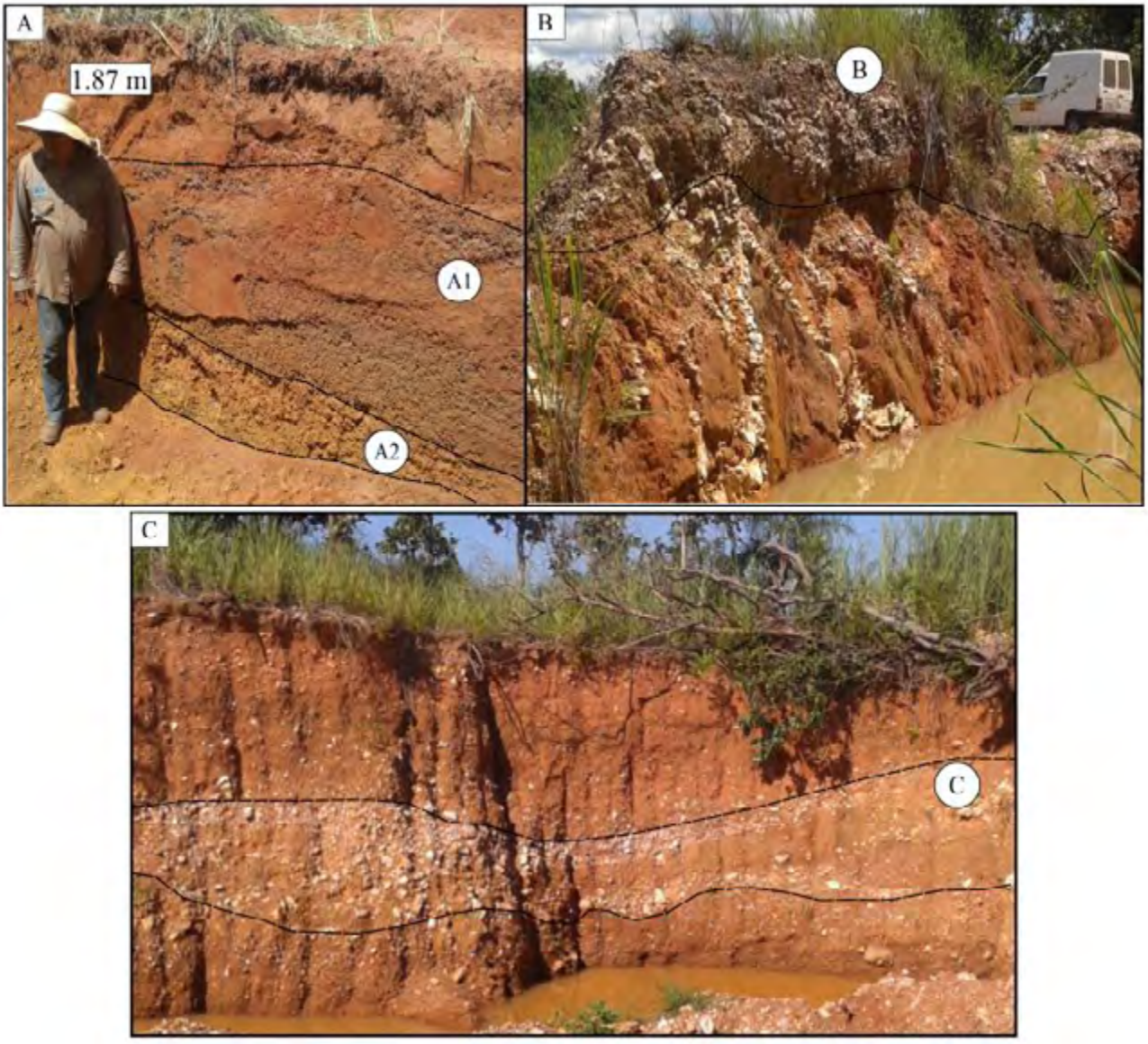

Figure 3 Detailed photographs of the locations marked on Figure 1 as each gravely levels position; A. gravel A1 (gray gravel) and A2 (yellowish gravel under gravel A1); B. gravel B located at the top of quartz veins; C. gravel C.

evaluation, the mean electromagnetic wave velocities for each layer were calculated, as shown in Table 2.

3 Results and Discussion

In this study, several survey lines were carried out until the best correlation between the open pit and the corresponding reflection pattern were found. Here, the locations of three of these lines is given, and its results are presented, since its more than enough to express the scope of this study. Each one of this three lines presented here intended to map a distinct gravel (A, B and C) that conferred with the secondary deposit's typical characteristics (alluvium, eluvium and colluvium) where gold is explored in this region. Six distinct reflection patterns were found. Where line 1 presented the reflection patterns 1 referring to the soil, and 2 referring to gravel B; line 2 presented the reflection patterns 3 referring to gravel C, and 4 referring to saprolite; and line 3 presented the reflection patterns 5 referring to gravel A1, and 6 referring to gravel A2.

Anuário do Instituto de Geociências - UFRJ
ISSN 0101-9759 e-ISSN 1982-3908 - Vol. 43 - 3 / 2020 p. 84-97

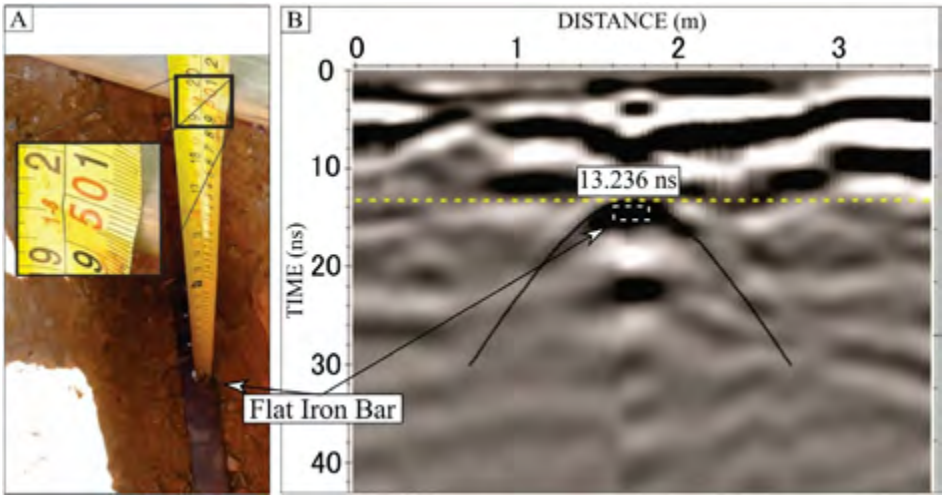

Figure 4 Electromagnetic wave's velocity calibration in the studied environment; A. photograph of flat iron bar buried at 0.5 m depth; B. screen capture of GPR data from the buried flat iron bar at 0.5 m depth, highlighting the dual time travel of 13.236 ns

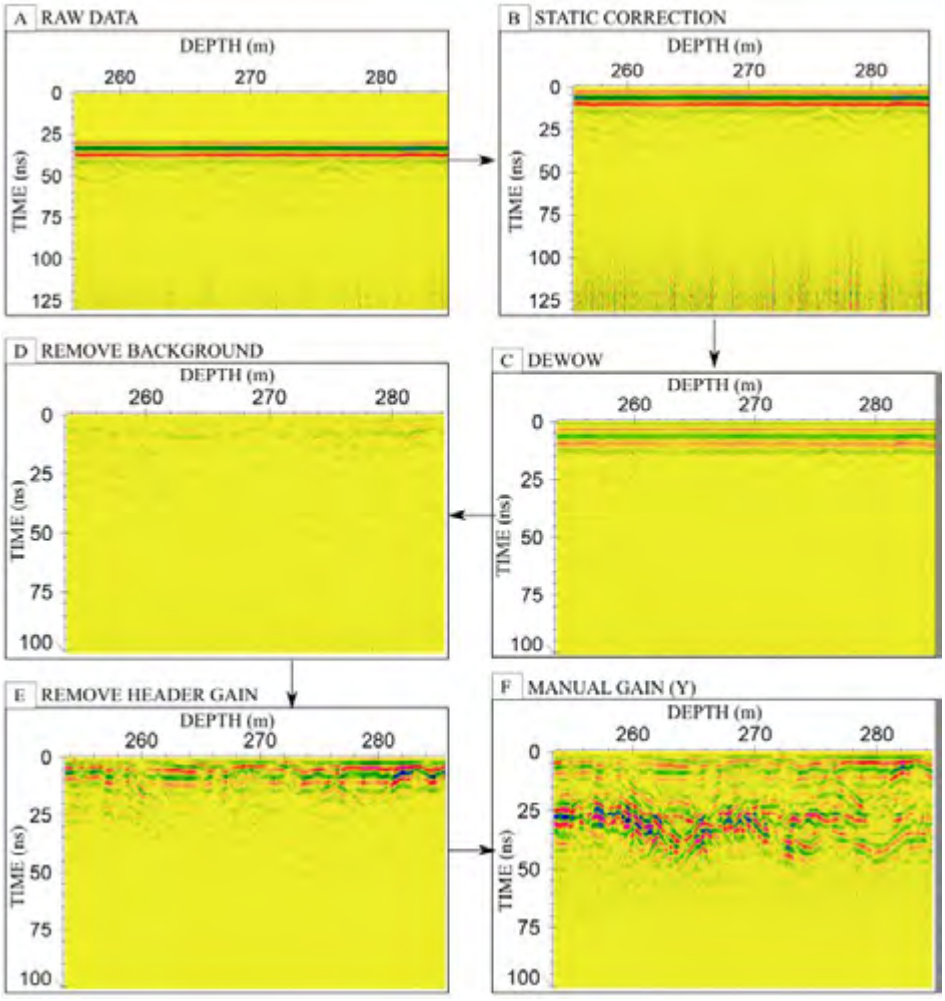

Figure 5 Schematic data processing flowchart; A. line 1 raw data; B. time-zero correction; C. dewow subtraction; D. background removal; E. header gain removal; F. manual gain (10 dB) along the y axis starting in 5 ns.

Gravel	Δs (m)	2Δt (ns)	Estimated Velocity (m/ns)	V1 (m/ns)	V2 (m/ns)	Mean Velocity (m/ns)
A1	1.62	37	0.087	0.08	0.09	0.086
A2	1.56	36	0.086	0.08	0.09	0.085
B	1.65	36	0.091	0.08	0.1	0.090
C	3.07	41	0.149	0.12	0.17	0.146

Table 2 Gravely level's estimated velocities. Δs: spatial interval (m); Δt: double travel time interval in each layer (ns); Estimated Velocity: velocity calculated from the estimated depths (m/ns); V1 and V2: minimum and maximum velocity for lithologies 1 and 2, respectively, observed with ReflexW (m/ns); Mean Velocity: velocity obtained by averaging the previous three velocities (m/ns).

The reflection patterns generally present high homogeneity and velocity along the gravely layers. They usually perform great amplitude occurrence between the values of -0.2 and +0.2 in the amplitude's histograms; and maximum values of -0.8 and 0.8. Their semi variograms commonly displayed smooth dips, with the reflection pattern 1 (Figures 6 and 7) semi variogram for soil being the mildest of all; the most inclined ones are related to reflection patterns 3 and 4, indicating a chaotic environment for line 2. After a lag distance of 1.9 (Figure 7), the variance line relative to reflection pattern 1 shows that there is no more correlation between its pattern data points, expounding the value of approximately 2×10^7. This pattern corresponds to the soil above gravel B, presenting itself predominantly discontinuous, with chaotic reflections and no apparent dip, which can be inferred a good correlation between its response and a sandy soil with the presence of clasts. It also presents lower amplitude values, ranging between -0.4 to 0.4, suggesting a signal attenuation, perhaps due to its soil clayey contents.

Reflection pattern 2 (Figures 6 and 7) is associated with gravely level B, which is a matrix-supported and poorly selected gravel, mainly formed by coarse and angulous clasts, probably some of those clasts were present in the soil above its layer, and gave rise to the chaotic reflections in the pattern 1. Pattern 2 has meandering and slightly wavy forms, presenting at some points chaotic and discontinuous reflections, this form agrees with Beres

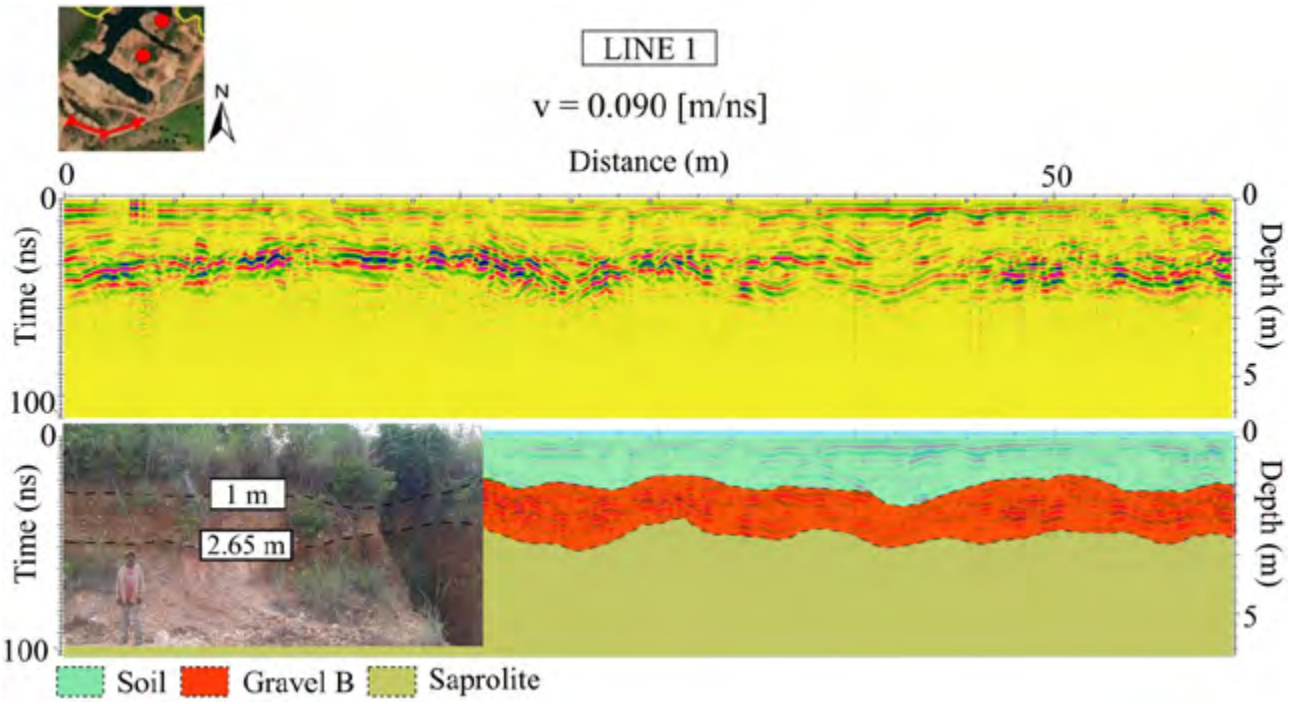

Figure 6 Capture illustrating the processed data obtained on line 1, the mean electromagnetic wave velocity, followed by its stratigraphic interpretation, with reflections continuity demarcation and its relationship with gravely level B.

Anuário do Instituto de Geociências - UFRJ
ISSN 0101-9759 e-ISSN 1982-3908 - Vol. 43 - 3 / 2020 p. 84-97

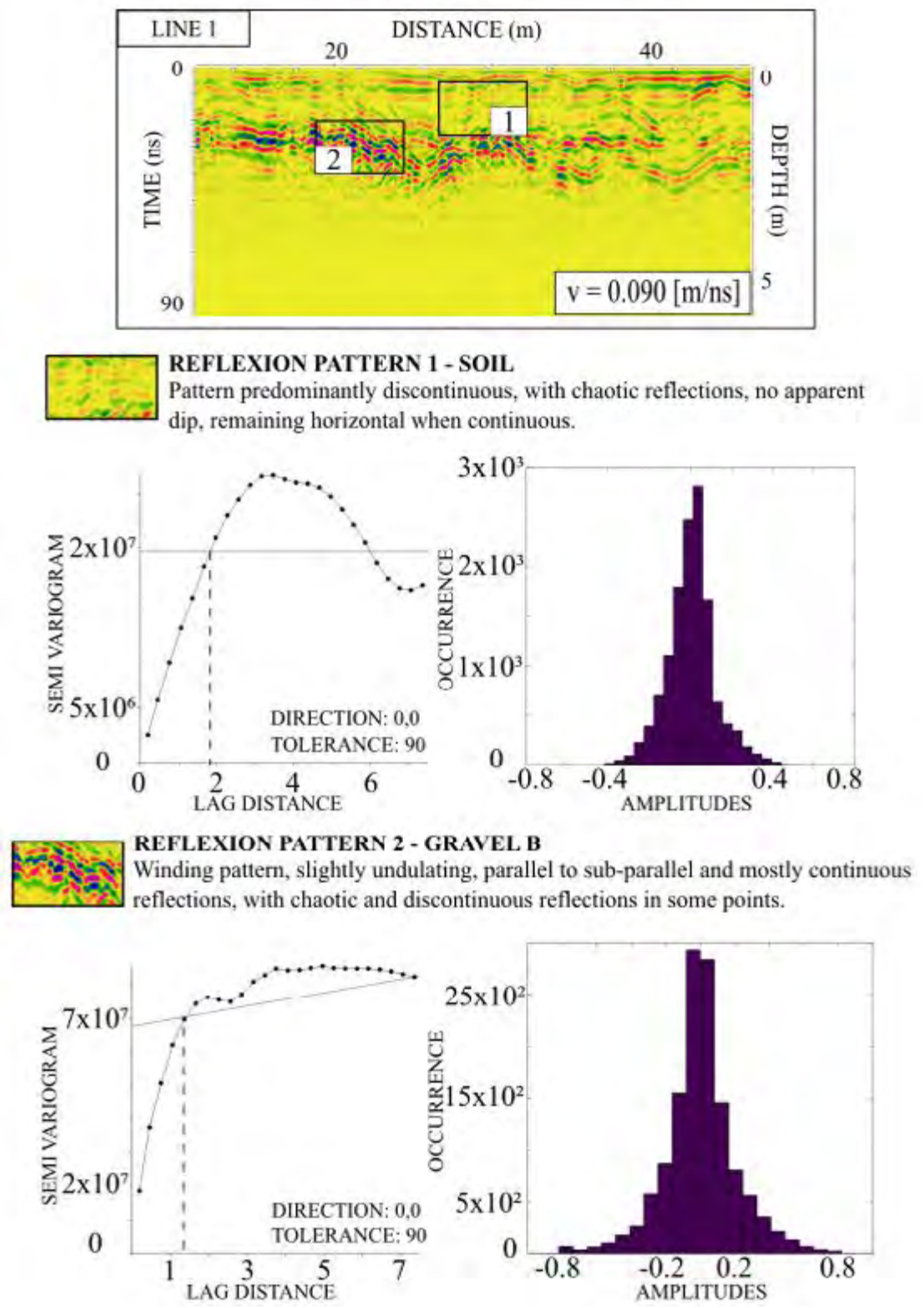

Figure 7 Capture illustrating the reflection patterns present in the processed data from the line 1, followed by their lithological correlations, descriptions and statistical data: semi variogram distribution by the lag distance and the variance line of approximately 2×10^7 for soil, and 7×10^7 for gravely level B; followed by its amplitude's histogram.

& Haeni (1991) description for sands and gravels. The calculated electromagnetic wave mean velocity for this layer is approximately 0.090 m/ns (Table 2), the second highest speed of this study, the first being that of gravely level C. This velocity is close to that related to dry sands, shale, saturated silts and mixed soil components saturated. After a lag distance of 1.4 (Figure 7), the variance line point to the end of correlation between this data points, expounding the value of approximately 7×10^7. Hence, the statistical analysis shows a more heterogeneous and chaotic amplitudes distribution, if compared with pattern 1, which can be related to the presence of poorly selected clasts. It presents higher amplitude values, ranging between -0.8 to 0.8, showing a good signal response, despite its higher depth if compared with reflection pattern 1 and this previous layer signal attenuation.

Reflection pattern 3 (Figures 8 and 9) is associated with gravely level C, a matrix-supported gravel, angulous and poorly selected, ranging from silt to cobbles. This pattern has alternating winding and chaotic reflections, agreeing as expected for isolated block gravel and sand (Beres & Haeni, 1991). This reflections form alternation may be related to the clast's heterogeneous distribution along the gravely layer. The calculated electromagnetic wave mean velocity for this gravely level is 0.146 m/ns, the highest velocity obtained in this study. This value match those related to sands and gravels, clays and sandy soils velocities. This pattern generated a well-inclined variogram, a variance line starting at the value of 45×10^6 matching the semi variogram curve in a lag distance of 2, indicating the end of correlation between the data points. Those statistical results announce sudden variations in the amplitude values, but a greater correlation between its data; it can be said that reflection pattern 3 have a greater continuous "chaotic behavior" if compared with the others reflection pattern. It presents higher amplitude values, ranging between -0.8 to 0.8, but most of its amplitudes are ranging between -0.2 to 0.2, showing great heterogeneity of the signal response along this layer, which confirms the "chaotic behavior".

Reflection pattern 4 refers to the saprolite (Figures 8 and 9). It has wavy reflections, with a dip to the right, its amplitudes have a higher occurrence between values of -0.1 to 0.1, which suggest a signal attenuation. The semi variogram for this data, observing the abscissa axis, has a smoother initial dip if compared to the previous reflection pattern, showing a greater spatial continuity in its amplitudes. After a lag distance of 1.6, the variance line starting at the value of 17×10^5 pointed to the end of correlation between the data points. Pattern 4 has a continuity similar to that of patterns 1 and 2 and less than that of pattern 3, even though its amplitudes are lower than all of those previous patterns; which may be related to the signal attenuation by depth or by some chemical component in this layer.

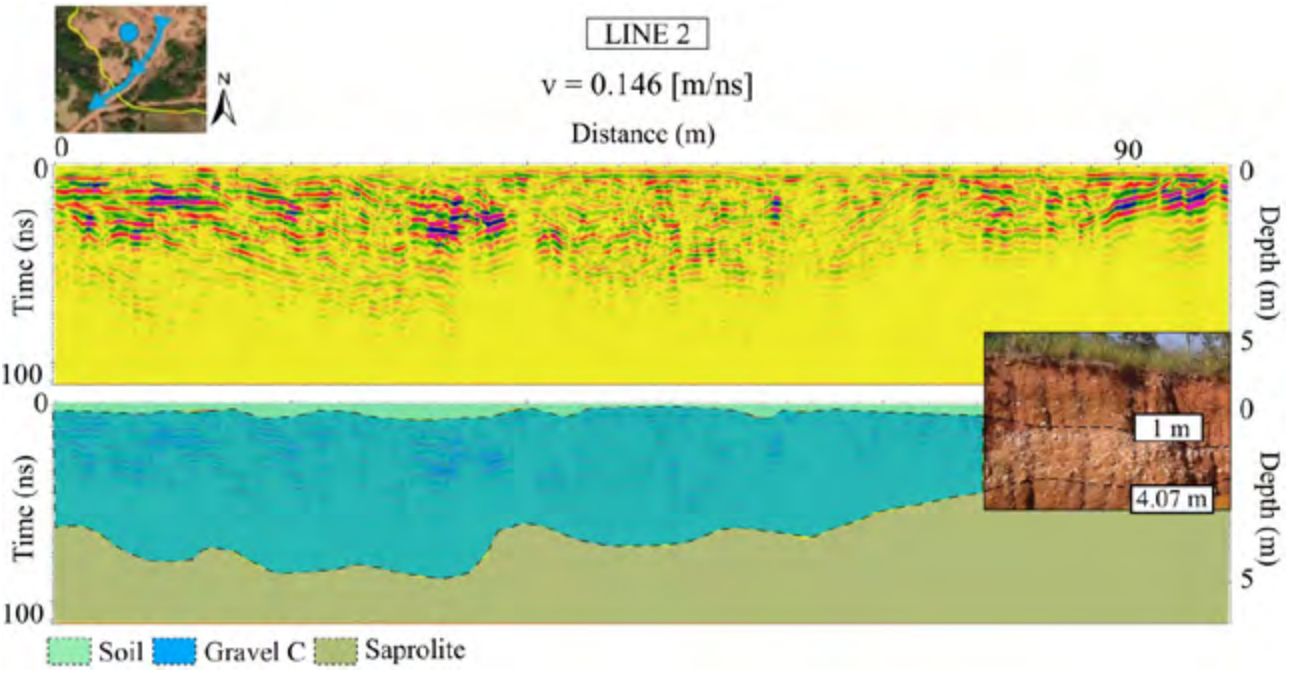

Figure 8 Capture illustrating the processed data obtained on line 2 profile, the mean electromagnetic wave velocity, followed by its stratigraphic interpretation, with reflections continuity demarcation and its relationship with gravely level C.

Anuário do Instituto de Geociências - UFRJ
ISSN 0101-9759 e-ISSN 1982-3908 - Vol. 43 - 3 / 2020 p. 84-97

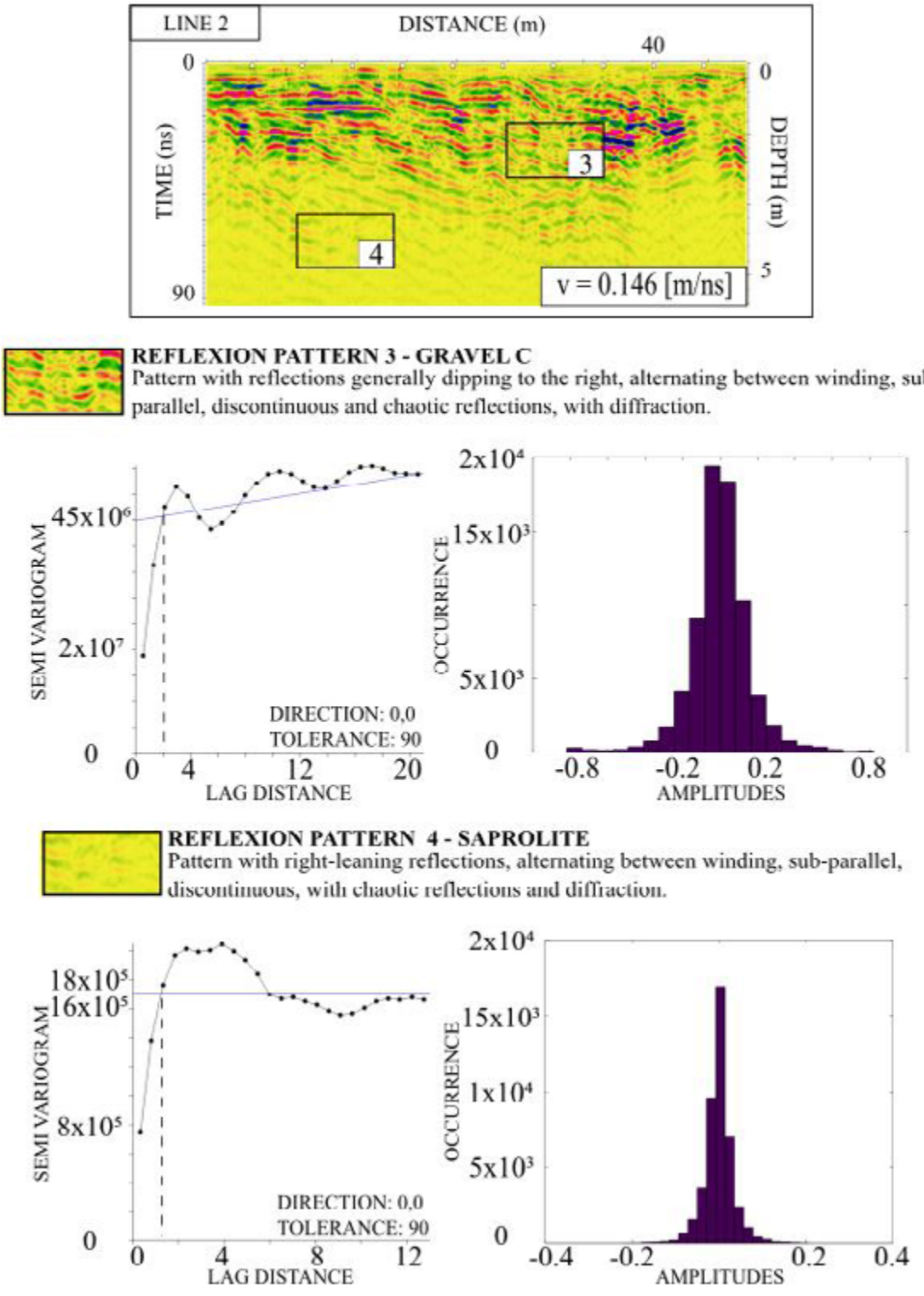

Figure 9 Capture illustrating the reflection patterns present in the processed data from the line 2, followed by their lithological correlations, descriptions and statistical data: semi variogram distribution by the lag distance and the variance line of approximately 45×10^6 for gravely level C, and 17×10^5 for saprolite; followed by its amplitude's histogram.

Reflection pattern 5 (Figures 10 and 11) is associated with gravely level A1, a matrix-supported gravel, mainly composed by fine particles of silt and clay together with larger and commonly rounded particles of sand and gravel, with the likely presence of hematite, which can give it a grayish color. This pattern has continuous and discontinuous reflections, alternating chaotic diffraction with meandering and sub-parallel reflections, in line with the expected pattern for sands and gravel (Beres & Haeni, 1991). The calculated electromagnetic wave mean velocity for this gravely layer is 0.086 m/ns. This velocity approximates to that obtained in sands, clays, silt and soils with saturated components. This pattern also presented a well inclined variogram with a variance line starting at the value of 13×10^7, matching the semi variogram curve in a lag distance of 1.7. Those statistical results announce sudden variations in the amplitude values, but a continuity similar to those of patterns 1 and 4, which matches with its gravel well selected clasts. Its amplitudes are mainly concentrated between the values of -0.2 and 0.2, even though reach higher values of -0.8 and 0.8, indicating good signal response.

The reflection pattern 6 (Figures 10 and 11) is associated with the gravely level A2, a matrix-supported, small and well selected gravel, with the likely presence of goethite, which can give it the yellowish tone. This pattern is predominantly reflection-free, with strong, meandering, sub-parallel and continuous reflection at its bottom, indicating a contrast between this layer and its underlayer. The calculated electromagnetic wave mean velocity for this gravely level is 0.085 m/ns. This value is very close to those of pattern 5, suggesting that the distinct chemical compositions of these materials cause no observed effect on the electromagnetic wave's velocity. Pattern 6 also presented a well inclined variogram with the variance line starting in the value of 3×10^7, and matching the semi variogram curve in a lag distance of 1.6. This statistical data indicates sudden variations in values and less continuity if compared to pattern 5. Its amplitudes reach values of -0.6 and 0.6, presenting a lower signal response if compared with the previous pattern. This may be related to the signal attenuation by depth or by some chemical component in this layer.

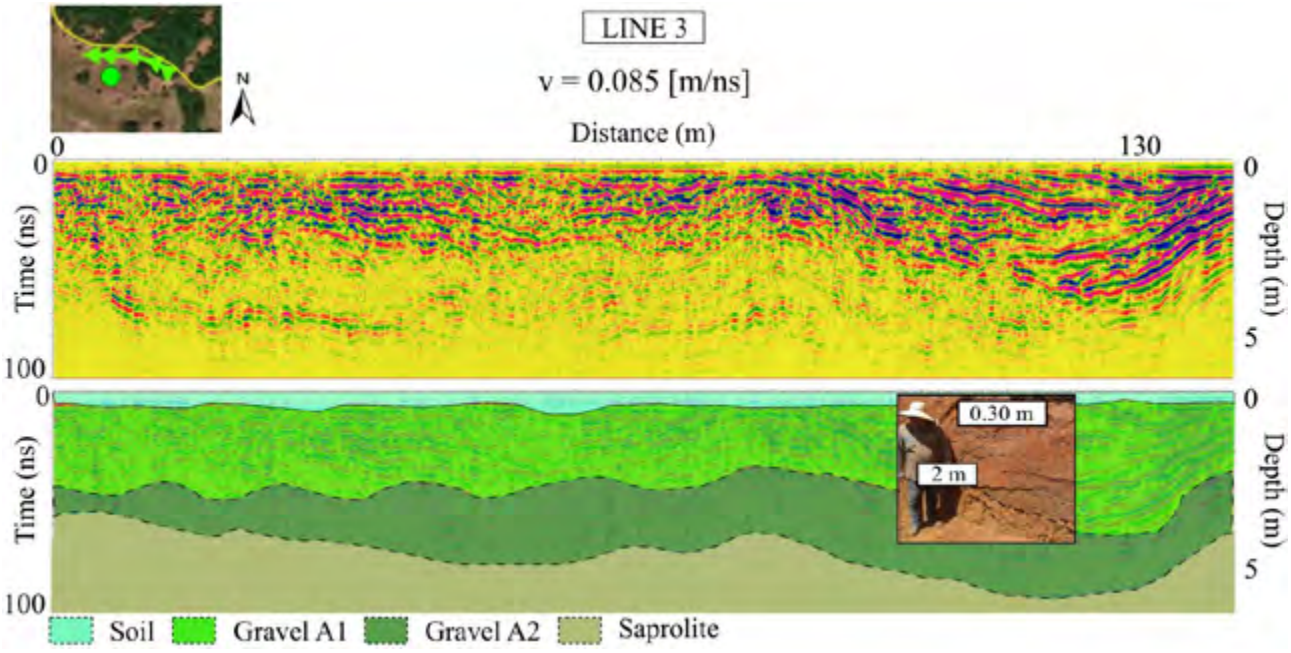

Figure 10 Capture illustrating the processed data obtained on line 3 profile, the mean electromagnetic wave velocity, followed by its stratigraphic interpretation, with reflections continuity demarcation and its relationship with gravely levels A1 and A2.

Anuário do Instituto de Geociências - UFRJ
ISSN 0101-9759 e-ISSN 1982-3908 - Vol. 43 - 3 / 2020 p. 84-97

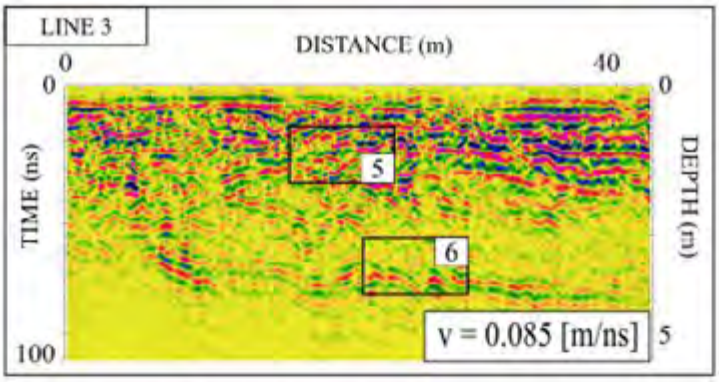

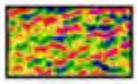

REFLEXION PATTERN 5 - GRAVEL A1

Pattern with continuous and discontinuous reflections, with alternating chaotic diffraction with horizontal, winding, and sub-parallel reflections.

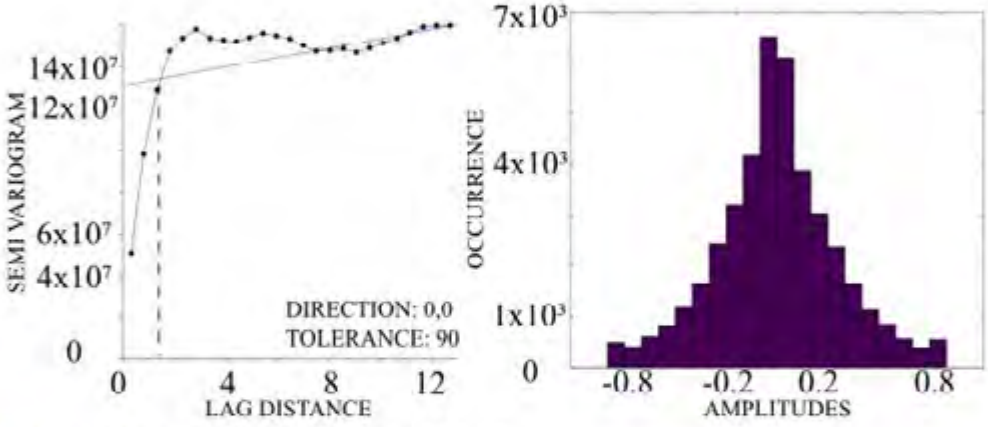

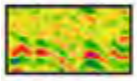

REFLEXION PATTERN 6 - GRAVEL A2

Predominantly reflection-free pattern, occurring on the underside of meandering, slightly undulating reflections, parallel and sub-parallel to horizontal with reflections mainly continuous.

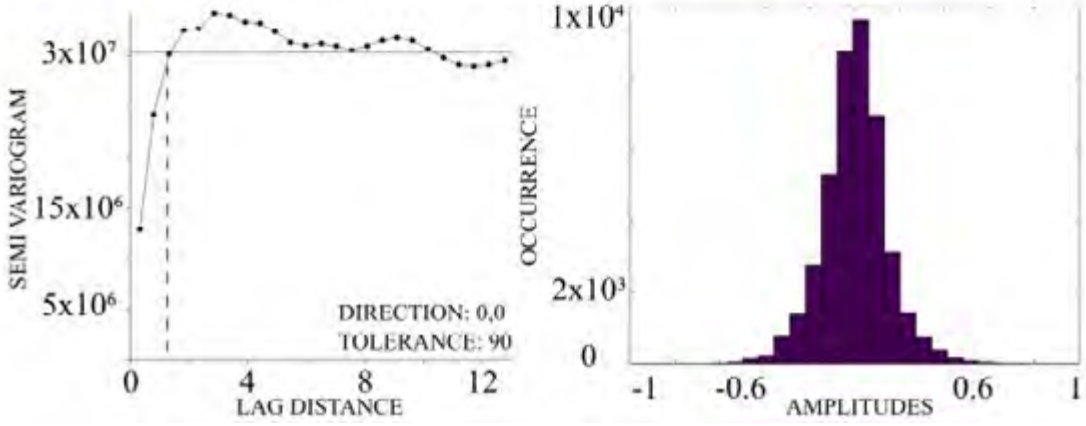

Figure 11 Capture illustrating the reflection patterns present in the processed data from the line 3, followed by their lithological correlations, descriptions and statistical data: semi variogram distribution by the lag distance and the variance line starting in the value of 13×10^7 for gravely level A1 and 3×10^7 for A2; followed by its amplitude's histogram.

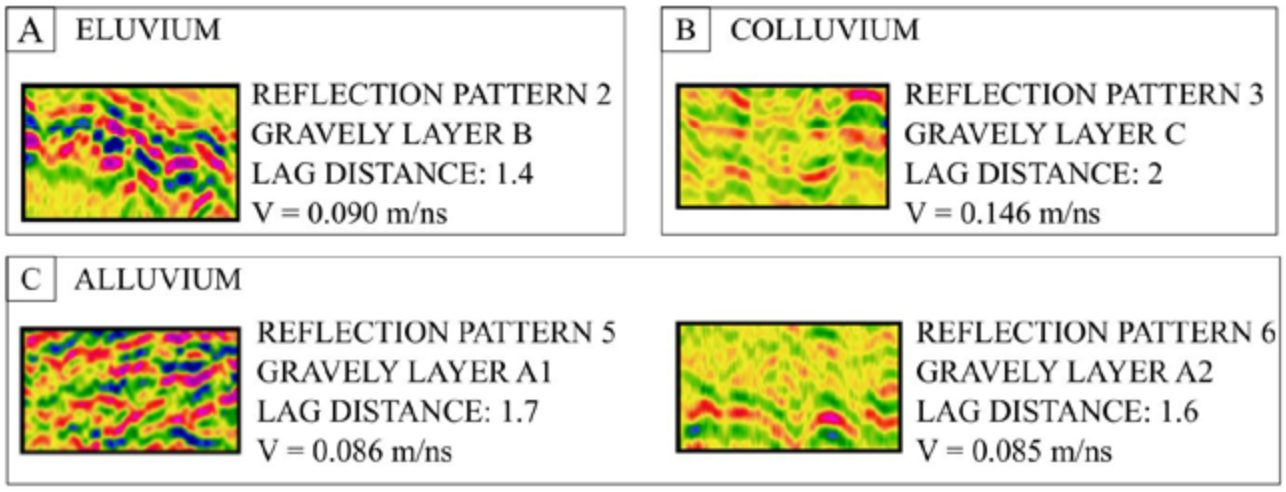

Figure 12 Screen capture illustrating: A. reflection pattern 2, related to gravely layer B, its lag distance, mean velocity and correlation with eluvium deposits; B. reflection pattern 3, related to gravely layer C, its lag distance, mean velocity and correlation with colluvium deposits; C. reflection pattern 5 and 6, related to gravely layer A1 and A2, respectively, its lag distance, mean velocities and correlation with alluvium deposits.

4 Conclusions

Some of these differences favor the possibility that gravels from these areas correspond to secondary deposits of different types. Where gravels A1 and A2, with its lower velocities and good signal response, would corresponds to an alluvium deposit; gravel B, with its presented statistical medium results, corresponds to an eluvium deposit; and gravel C, with its higher velocity, and greater distance lag, to a colluvium deposit. Figure 12 summarizes this interpretation.

The GPR data presented excellent results regarding the correlation between grain size, reflection patterns, wave velocity in the medium and statistical analysis, being consistent with the theory and the observed layers in the field. The set of investigations carried out in the surveyed areas indicate that GPR is an efficient method to discriminate secondary deposits. However, despite the GPR data perform great difference in its result to each layer; the statistical similarities in the responses for gravel A1 and A2 bring to light the ambiguity of this method capacity in differentiate deposits with great physical similarities and some chemical differences. Although, statistical analysis and visual descriptions, can work together to assess GPR data reflection patterns.

5 Acknowledgments

This research was supported by the University of Brasilia Geography Department, Geochemistry Laboratory (LAGEQ) and Applied Geophysics Laboratory (LGA). The Project were financial supported by Isma Maria Dorilêo Ferreira de Assis's mining. The authors thank Bruno Nascimento Ferreira, Remke van Dam and Rogério Elias Soares Uagoda, as well as the reviewers of this paper, for their useful comments and suggestions.

6 References

Alvarenga, C.J.S. & Trompette, R. 1993. Brasiliano tectonic of the Paraguay Belt: the structural development of the Cuiabá region. *Revista Brasileira de Geociências*, *23*: 18-30.

Barboza, E.S. 2008. *Gênese e controle estrutural das mineralizações Auríferas do Grupo Cuiabá, na Província Cuiabá-Poconé, centro Sul do Estado de Mato Grosso–Brasil.* Faculdade de Geologia, Universidade do Estado do Rio de Janeiro, Tese de Doutorado, 155p.

Beres Jr, M. & Haeni, F.P. 1991. Application of ground-penetrating-radar Methods in Hydrogeologie Studies. *Groundwater, 29*(3): 375-386.

Beres, M.; Green, A.; Huggenberger, P. & Horstmeyer, H. 1995. Mapping the architecture of glaciofluvial sediments with three-dimensional georadar. *Geology*, *23*(12): 1087-1090.

Bersezio, R.; Giudici, M. & Mele, M. 2007. Combining sedimentological and geophysical data for high-resolution 3-D mapping of fluvial architectural elements in the Quaternary Po plain (Italy). *Sedimentary Geology*, *202*(1-2): 230-248.

Calder, M. & Kennedy, D.M. 2013. The Application of Ground Penetrating Radar in Delineating Shore Platform Morphology: A Case Study from Wellington, New Zealand. *Journal of Coastal Research, 29*(6a): 226-234.

Chen, D.L.; Huang, C.L. & Su, Y.A. 2004. An integrated method of statistical method and Hough transform for GPR targets detection and location. *Acta Electronica Sinica*, *32*(9): 1468-1471.

Davis, J.L.; Annan, A.P. & Vaughan, C.J. 1984. Placer exploration using radar and seismic methods. *In*: SEG TECHNICAL PROGRAM EXPANDED ABSTRACTS, 1984. Society of Exploration Geophysicists, p. 306-308.

Del'Rey Silva, L.J.H. 1990. Ouro no Grupo Cuiabá, Mato Grosso: contrôles estruturais e implicações tectônicas. *In*: CONGRESSO BRASILEIRO DE GEOLOGIA, Vol. *36*, No. 6, 1990.

do Couto Tokashiki, C. & Saes, G.S. 2008. Revisão estratigrafica e faciologia do Grupo Cuiabá no alinhamento Cangas-Poconé, baixada Cuiabana, Mato Grosso. *Revista brasileira de Geociências, 38*(4): 661-675.

Engdahl, N.B.; Weissmann, G.S. & Bonal, N.D. 2010. An integrated approach to shallow aquifer characterization: combining geophysics and geostatistics. *Computational Geosciences, 14*(2): 217-229.

Fernandes, J.C. & Miranda, J.G. 2006. Províncias e distritos auríferos do mato grosso: Produção garimpeira e industrial. *In:* VIANA, F. (ed.). *Coletânea Geológica do Mato Grosso*., Editora UFMT, 2:p. 07-33.

Ferreira Filho, O.B. 2019. Anuário Mineral Brasileiro: Principais Substâncias Metálicas - Ano Base 2017. *In*: Anuário Mineral Brasileiro, Brasília, Brasil, Agência Nacional de Mineração (ANM), p. 34.

Francké, J.C. & Yelf, R. 2003. Applications of GPR for surface mining. *In*: PROCEEDINGS OF THE 2ND INTERNATIONAL WORKSHOP ON ADVANCED GROUND PENETRATING RADAR, 2003. IEEE, p. 115-119.

Heinz, J.; Kleineidam, S.; Teutsch, G. & Aigner, T. 2003. Heterogeneity patterns of Quaternary glaciofluvial gravel bodies (SW-Germany): application to hydrogeology. *Sedimentary geology, 158*(1-2): 1-23.

Huggenberger, P.; Meier, E. & Pugin, A. 1994. Ground-probing radar as a tool for heterogeneity estimation in gravel deposits: advances in data-processing and facies analysis. *Journal of Applied Geophysics, 31*(1-4): 171-184.

Kostic, B.; Becht, A. & Aigner, T. 2005. 3-D sedimentary architecture of a Quaternary gravel delta (SW-Germany): Implications for hydrostratigraphy. *Sedimentary Geology, 181*(3-4): 147-171.

Luz, J.S.; Oliveira, A.M.; Souza, J.O.; Motta, J.J.I.M.; Tanno, L.C.; Carmo, L.S. & Souza, N.B. 1980. Projeto Coxipó–relatório Final. Companhia de Pesquisa de Recursos Minerais. Superintendência Regional de Goiânia. *DNPM CPRM*, *1*: 136.

Moysey, S.; Knight, R.J. & Jol, H.M. 2006. Texture-based classification of ground-penetrating radar images. *Geophysics, 71*(6): K111-K118.

Neal, A. 2004. Ground-penetrating radar and its use in sedimentology: principles, problems and progress. *Earth-science reviews, 66*(3-4): 261-330.

Pires, F.R.M.; Gonçalves, F.T.T.; Ribeiro, L.A.S. & Siqueira, A.J.B. 1986. Controle das mineralizações auríferas do Grupo Cuiabá, Mato Grosso. *In*: CONGRESSO BRASILEIRO DE GEOLOGIA, Vol. *34,* p. 2383-2395, 1986.

Pueyo Anchuela, Ó.; Luzón, A.; Pérez, A.; Muñoz, A.; Mayayo, M.J. & Gil Garbi, H. 2016. Ground penetrating radar evaluation of the internal structure of fluvial tufa deposits (Dévanos-Añavieja system, NE Spain): an approach to different scales of heterogeneity. *Geophysical Journal International*, *206*(1): 557-573.

Rauber, M.; Stauffer, F.; Huggenberger, P. & Dracos, T. 1998. A numerical three-dimensional conditioned/unconditioned stochastic facies type model applied to a remediation well system. *Water Resources Research*, *34*(9): 2225-2233.

Regli, C.; Huggenberger, P. & Rauber, M. 2002. Interpretation of drill core and georadar data of coarse gravel deposits. *Journal of Hydrology, 255*(1-4): 234-252.

Sandmeier, K.J. 2011. Reflexw 6.0 Manual Sandmeier Software, Karlsruhe. Available in: <https://www.sandmeier-geo.de/>.

Silva, C.H.; Simões, L.S.A. & Ruiz, A.S. 2016. Caracterização estrutural dos veios de quartzo auríferos da região de Cuiabá (MT). *Revista Brasileira de Geociências*, *32*(4): 407-418.

Tebchrany, E.; Sagnard, F.; Baltazart, V.; Tarel, J.P. & Derobert, X. 2014. Assessment of statistical-based clutter reduction techniques on ground-coupled GPR data for the detection of buried objects in soils. *In*: PROCEEDINGS OF THE 15TH INTERNATIONAL CONFERENCE ON GROUND PENETRATING RADAR, 2014. IEEE, p. 604-609.

Vandenberghe, J. & Van Overmeeren, R.A. 1999. Ground penetrating radar images of selected fluvial deposits in the Netherlands. *Sedimentary Geology, 128*(3-4): 245-270.

Watts, A. & Gubins, A.G. 1997. Exploring for nickel in the 90s, or 'til depth us do par'. *In*: PROCEEDINGS OF EXPLORATION, Vol. *97*, p. 1003-1014, 1997.